Power and Accuracy Optimization for Luminescent Transcutaneous Oxygen Measurements

Burak Kahraman*, Ian Costanzo*, Neal Kurfis[†], Guixue Bu[†], Jiayuan Wang[†],
Foroohar Foroozan[†], and Ulkuhan Guler*

*Department of Electrical and Computer Engineering, Worcester Polytechnic Institute, Worcester, MA 01609 USA

[†]Analog Devices Inc., Wilmington, MA 01887 USA

Abstract—Transcutaneous oxygen sensing is a noninvasive method for continuous monitoring of partial pressure of oxygen diffused through the skin that closely correlates with changes in arterial blood gases. A method for measuring transcutaneous oxygen, suitable for a wearable device, is luminescence oxygen sensing. This study aims to determine the optimum values of the system parameters for power, accuracy, and precision for the development of transcutaneous oxygen wearable based on a platinum-porphyrin film and the ADPD4101 analog front-end. For this purpose, we conducted several experiments using the CN0503 optical measurement system from Analog Devices, Inc. Based on the optimization experiments, we determined a 100 mA and 100 μ s LED pulse intensity and width, and a 2 μ s sampling period gave a good compromise between power and signal integrity. Using these settings, we observed a discernible τ response to changes in oxygen pressure from 0 to 418 mmHg.

I. Introduction

Respiratory diseases are among the leading causes of death and disability, imposing an enormous worldwide health burden [1]. About one in twelve Americans have asthma, a lifelong disease, with an increasing rate every year [2]. Adults with chronic obstructive pulmonary disease (COPD) and other respiratory issues constitute 4 to 12% of the population of the U.S [3]. Respiratory distress is one of the most common reasons infants are admitted into the neonatal intensive care unit (NICU) [4]. Fortunately, with proper care and medication in a living environment, most patients with respiratory diseases can control their symptoms and prevent severe conditions [5].

The effectiveness of respiration—inhaling in oxygen (O₂), oxygenation, and exhaling out carbon dioxide (CO₂), ventilation—is measured by blood gases. Medical professionals monitor blood gas content using bulky bedside instruments, typically in eight hour intervals [6]. However, it is not feasible to use this system in a home environment. These clinical instruments are expensive and it is difficult for medical professionals to remotely access the collected respiration data [7]. An inexpensive, miniaturized, wearable device—that can continuously monitor blood gases and securely transmit data to clinical experts—would enable safer and more effective treatment of respiratory diseases in a home environment.

A noninvasive technique of measuring blood gases is transcutaneous monitoring, which measures blood O_2 and CO_2 that are diffused through the skin. Changes in transcutaneous O_2 and CO_2 can directly correlate with changes in gases in the blood stream [8]–[10]. Our focus in this paper is measuring partial pressure of transcutaneous oxygen (PtcO₂).

Traditionally, PtcO₂ is measured using bulky electrochemical probes [11]. Recently, researchers have been exploring luminescence oxygen sensing techniques, leveraging moleculesensitive luminophore-dye sensors and optoelectronics, to enable miniaturized transcutaneous blood gas monitors [12]–[16]. However, the state-of-the-art is either invasive [17], [18] or immature prototype demonstrations [12]–[15], which requires further research to establish the technology.

Luminescente materials can be made selective such that its luminescence is quenched by a specific gas species (e.g., oxygen) [19]. In our case, we use a sensor composed of a platinum porphyrin dye in a polymer matrix. There is an inverse relationship between the concentration of O₂ and the intensity and decay time of the luminescence [19]. Decay time measurements are of particular interest as the luminescence time constant is decoupled from the excitation power and less sensitive to changes such as aging or dye density [7].

In this paper, we analyzed two measurement methodologies for luminescent oxygen sensing, investigating their accuracy and sensitivity while optimizing power consumption from a wearable device perspective. We performed experiments with the CN0503 optical platform from Analog Devices Inc. (ADI) [20]. Section II explains the data acquisition system and techniques to measure the sensor's decay time. Section III demonstrates the experiment environment and argues parameters considered system optimization. Section IV presents the experiment results and discusses the possible influences on the wearable design. Our findings are summarized in Section V.

II. DATA ACQUISITION SYSTEM

We have employed the CN0503 optical measurement system from ADI, to measure the luminescent decay time of the platinum-porphyrin sensor-film under various oxygen partial pressure conditions. The ADPD4101 is the core of the CN0503 platform, shown in the simplified schematic in Fig. 1. The ADPD4101 is a multimodal photometric analog front-end (AFE) with integrated LED drivers, dual channel signal conditioning path including transimpedance amplifier (TIA) and analog integrator for measuring signal from photodiodes (PD), analog to digital converter (ADC) and first-in-first-out (FIFO) memory to buffer the sample data. We explored two sampling methods to measure the decay time of the luminescent signals: impulse response (IR), and single-sided integration (SSI), adopted from ADI.

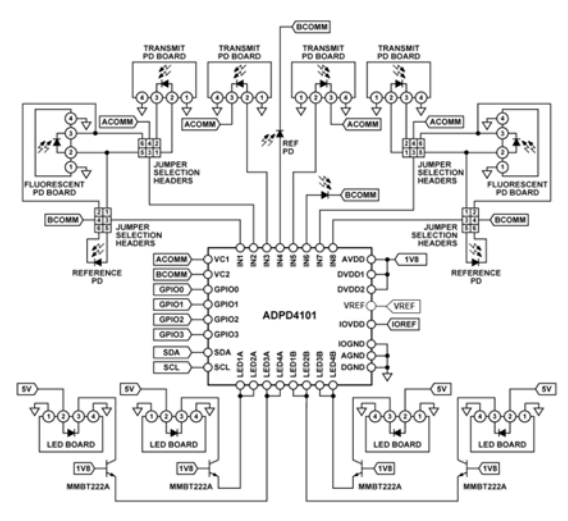


Fig. 1. Simplified schematic of the CN0503 [20].

A. Impulse Response Mode

In the IR mode, we excite the sensor with a single LED pulse, and take successive samples of the luminescent decay curve in an acquisition window following the end of the LED pulse, illustrated in Fig. 2a. The LED pulse width, the sampling period, and the acquisition window are user specified parameters. The sampling period is limited to minimum of 2 μ s due to timing limitations of FIFO in ADPD4101 in this mode. τ is calculated as follows. If the decay curve is

$$v(t) = Ae^{-t/\tau},\tag{1}$$

then, the sample produced by the IR mode with sampling period of n at time t will be

$$sample(t) = Ae^{-t/\tau} + Ae^{-(t+n)/\tau} = A(1 + e^{-n/\tau})e^{-t/\tau}.$$
 (2)

Then, we can recover original decay curve as

$$y(t) = \frac{sample(t)}{1 + e^{-n/\tau}}. (3)$$

Finally, we use Eq. 3 and the least squares method, to calculate A and τ . These steps are repeated and averaged to reduce noise.

B. Single Sided Integration Mode

The SSI mode employs a supersampling strategy to improve the temporal resolution of the acquired luminescent decay curve. The sampling of the decay curve is performed by employing the following procedure, also illustrated in Fig. 2b. First, pulse the LED with a user specified LED pulse width. Next, integrate the signal from the PD starting at the user specified integration offset point from the end of the LED pulse and continue for predetermined integration width of 8 μ s. This gives the first sample point of the decay curve. For the next sample point of the decay curve, repeat the LED pulse, but the integration offset is increased by the user defined temporal resolution. Repeat this "LED-pulse-then-integration" sequence until the integration offset is greater than or equal to the user specified acquisition width (time period in which we take samples from the decay curve).

The procedure for reconstructing the decay curve and calculating its time constant in SSI mode is as follows. If the true

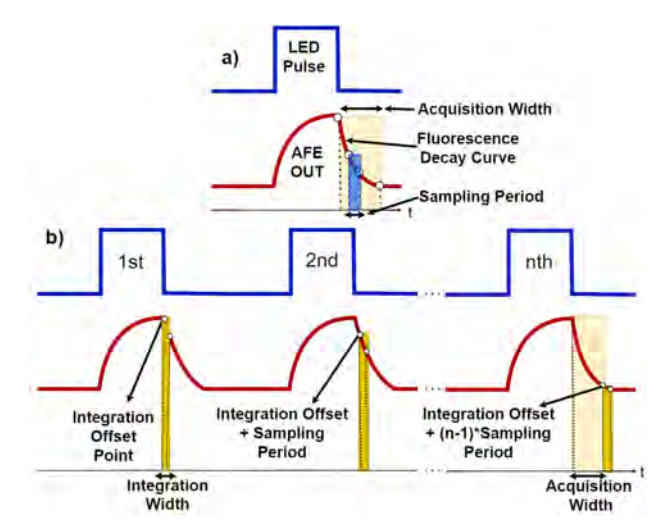


Fig. 2. Timing diagrams of a) IR mode and b) SSI mode.

decay curve is same as in the IR mode, sample produced by the SSI mode with integration width of L at time t will be

$$sample(t) = \int_{t}^{t+L} Ae^{-T/t} dT = A^{-t/\tau} (1 - e^{-L/t}).$$
 (4)

Then, we can recover original decay curve as

$$y(t) = \frac{sample(t)}{\tau(1 - e^{-L/t})}. (5)$$

Finally, using Eq. 5 and least squares method, the parameters A and τ are calculated like in the IR mode.

In SSI mode, the increment in integration offset can be as small as 31.25 ns. Thus, the SSI mode offers better temporal resolution compared to IR mode. In both of these modes, to reduce noise, the system takes the average over many trials. In terms of noise and power consumption, the IR mode offers the lowest noise and power consumption because each decay time measurement is done with one LED pulse, which eliminates the variation in the energy delivered to the luminophore from one LED pulse to the next. The SSI mode has higher power consumption and noise due to pulsing of the LED once per sample in a sequential order of multiple LED pulses.

III. EXPERIMENTAL SETUP

A. Signal Integrity and Analysis Setup

We first investigated the parameters for optimum power, accuracy, and precision of a luminescent decay time measurement system built around the ADPD4101. The goal of this experiment is to show the impact of measurement technique—SSI versus IR—on power requirements and measurement quality. These experiments were conducted at normal atmospheric conditions near sea level and at room temperature.

- 1) Sample preparation: The luminescent sensor is placed on a piece of black inflorescent paper. This paper is then placed inside a cuvette at an angle such that the sample has line of sight on the exciting LED and the photosensor.
- 2) Optical channel setup: The sample inside a cuvette is placed inside a holder in one of the optical channels of the CN0503. The exciting LED (L1C1-VLT1, Lumileds) is 430 nm, the wavelength sensitive to O_2 quenching, and

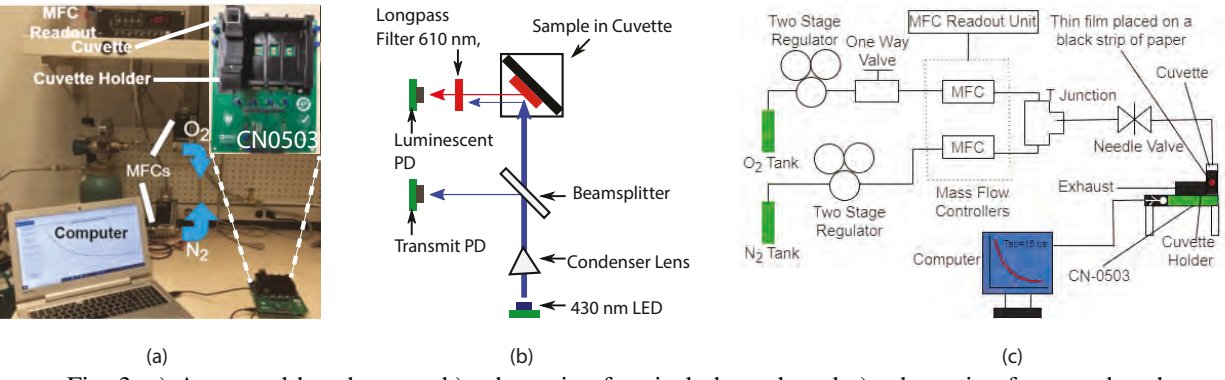


Fig. 3. a) Annotated bench setup, b) schematic of optical channel, and c) schematic of gas testbench.

the photosensor is a broad spectrum silicon photodiode (TEMD5080X01, Vishay) deployed an optical filter (SCHOTT RG-610, Edmund Optics) with a longpass characteristic at 610 nm, the emitting spectrum of the dye. The filter is placed in front of the photodiode's active area, illustrated in Fig. 3b.

3) Measurement and analysis setup: The data measured with the CN0503 platform is sent to a PC over a USB cable for post-processing and analysis. We took 2500 and 1000 decay time measurements for each LED pulse width and sampling period value for IR and SSI modes, respectively. The optical platform allows us to change the current from 0 to 400 mA. We then calculated the mean and standard deviation for each LED pulse width and current and sampling period. The obtained mean and standard deviation data points from the LED current analysis are fitted with a sigmoid and polynomial function, respectively.

B. Gas Measurements

The gas experiment setup is shown in Fig. 3a and is illustrated as a schematic in Fig. 3c. Oxygen (OX UHP20, Airgas) and nitrogen (NI UHP80, Airgas) are mixed at specific mass flow rates to precisely control the partial pressure of oxygen (PO₂) exposed to the sensor. Two MKS 1179A12CS1BV mass flow controllers (MFCs) and a MKS 247 mass flow control unit are used to set the mass flow rates, and thus the partial pressure of the test gases. We varied the PO₂ from 0 mmHg to 418 mmHg by changing the flow rate of oxygen from 0 standard cubic centimeters per minute (sccm) to 55 sccm while adjusting flow rate of nitrogen such that the sum of two flow rates equal to 100 sccm at each time. This range covers the typical values of PtcO₂ in humans, 50-120 mmHg.

IV. RESULTS AND DISCUSSION

A. Power Optimization Results

The LED pulse width, shown in Fig. 2, has a direct influence on the overall power consumption, as LEDs are one of the most power-hungry components on a wearable device. Thus, it is desirable to minimize the LED pulse width. On the other hand, the LED pulse needs to be on long enough to excite enough luminophores in the sensing dye to be able to obtain accurate measurements with a high signal to noise ratio. Therefore, the excitation duration should be optimized for accurate measurement and minimum power consumption.

We varied the LED pulse width from 20 μ s to 120 μ s in 10 μ s increments for both IR and SSI modes. The results of the experiments, presented in Fig. 4, indicate that the mean decay time shows an increase up to 100 μ s LED pulse width approaching an asymptote \sim 14.5 μ s after that point. Additionally, the effect of varying LED drive current on τ measurement in IR and SSI modes is presented in Fig. 5.

Thus, we can state that a LED pulse width as $100~\mu s$ is an optimization point for both IR and SSI modes. With that decision, the power consumption would be reduced to half compared to the work presented in [7], in which the miniaturized system was operated with $200~\mu s$ LED pulse width and the τ measured is similar in both experiments. For current optimization, 100~mA and 150~mA are where IR and SSI modes reach to asymptote, respectively. Increasing current beyond these values contributes to power consumption, with minimal improvement in signal quality.

B. Accuracy and Precision Optimization Results

The accuracy and precision of the sensor readings depend on how much readings deviate from the nominal τ value. Accuracy evaluates whether the average of a series of measurements has systematic error or bias. In our experiments, we use the mean, μ , for accuracy discussion. Similarly, the definition for precision is how much each measurement differs from another. The random error, σ , determines precision. Sampling rate and pulse width affect the σ and μ values.

For accuracy and precision optimization analysis, we have used the same setup as for power optimization. We vary the sampling period from 2 μs to 10 μs in IR mode and from 0.1 μs to 5 μs in SSI mode. The results of the experiment, presented in Fig. 6, show that as the sampling period decreases μ value converges \sim 14.5 μs in both modes.

In Fig. 4, the mean value settles around 90 μ s for both IR and SSI modes. We chose to drive the LED with a 100 μ s pulse width to ensure that the luminophores are fully excited and small variations in the LED pulse width do not translated to variations in the decay time.

In the sampling period analysis, the μ values concentrate in a narrower range for SSI mode compared to IR mode, because of the shorter effective sampling period that SSI mode can provide. In IR mode, the μ values in the sampling periods up to 5 μ s are very close to that of in the SSI mode, shown in

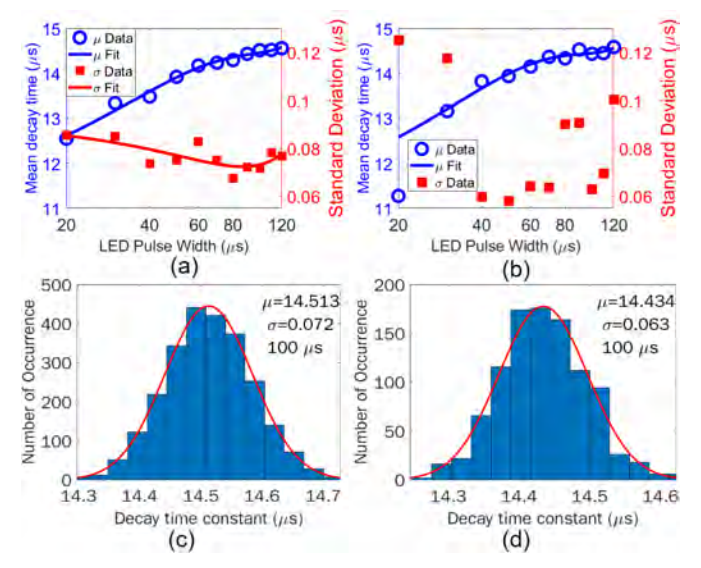


Fig. 4. Effects of LED pulse width on decay time measurement in a) IR mode, b) SSI mode and histogram of decay time measurement at 100 μ s in c) IR mode, d) SSI mode.

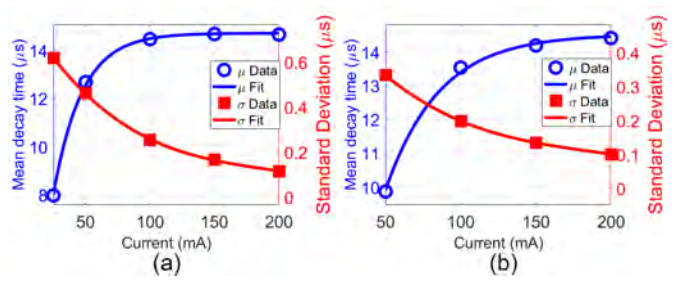


Fig. 5. Effects of LED drive current on decay time measurement in a) IR mode, b) SSI mode.

Fig. 6a. Based on these results, IR mode has competitive μ values at sampling periods lower than 5 μ , which makes IR mode our to go choice due to the lower power consumption accomplished in this mode. If very fast decay time need to be sampled, we can switch to SSI mode for better temporal resolution at the expense of higher power consumption.

Standard deviation results in pulse width and sampling rate analysis are used to assess the precision of both sampling techniques. In IR mode, the pulse width analysis showed a minimum σ of 0.063 μ s around 100 μ s LED pulse width. In the sampling rate analysis, σ drops as the sampling period decreases. Less than 0.1 μ s σ is obtained for the sampling periods lower than 10 μ s, depicted in Fig. 6c. For SSI mode, although σ does not show an obvious trend, the minimum σ is again around 100 μ s, shown in Fig. 4b. In the sampling period analysis, σ demonstrates an order of magnitude better precision in SSI mode than that of in IR mode.

C. Gas Experiment Results

We used IR mode with optimized parameters for measuring the decay time during the gas experiment. We took 1000 samples at each partial pressure value and calculated the statistical properties. The results are presented in Fig. 7. We

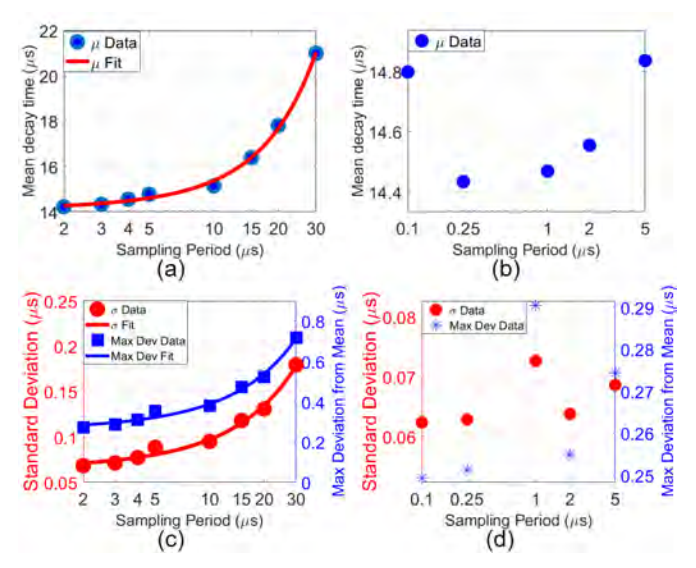


Fig. 6. Effects of sampling period on mean decay time in a) IR mode, b) SSI mode and on standard deviation and maximum deviation from mean in c) IR mode, d) SSI mode.

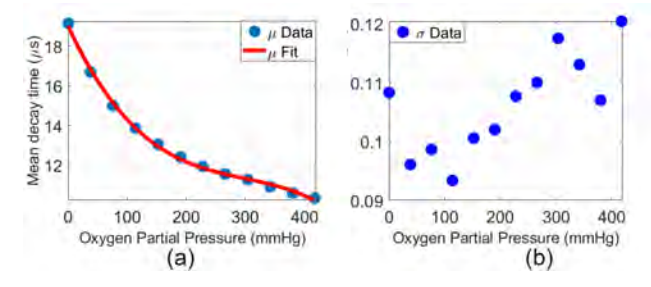


Fig. 7. For 0-418 mmHg, a) mean decay time, b) standard deviation.

measured decay time from 19 μ s to 10.3 μ s for PO₂ ranging from 0 to 418 mmHg, and the trend in mean decay time as PO₂ increases is similar to the work done in [7]. The calculated standard deviation is in the range of 0.09 μ s to 0.12 μ s.

To translate τ values in μ s to PtcO₂ values in mmHg, we leverage the gas experiment results, presented in Fig. 7. In the region which we are interested in, 50mmHg to 150mmHg, we will assume $\Delta \tau$ versus ΔPtcO_2 is linear. We have observed a change of 3.7 μ s in the decay time measured in the medically significant range. Hence, we will use $\frac{100mmHg}{3.7\mu s}$ as a conversion factor. In the worst case σ , the 0.12 μ s corresponds to 4.05% error, which is lower than the 6% allowable error required by the Food and Drug Administration (FDA) [21].

V. CONCLUSION

We performed experiments to determine the LED pulse width, LED current, and sampling period for power, accuracy, and precision optimization. We demonstrated that using IR mode with 2 μ s sampling period and 100 μ s LED pulse width with 100 mA LED current is an optimum choice for an accurate decay time measurement. We also showed, using these settings, the decay time measurements resolved the changes in the partial pressure of oxygen from 0 to 418 mmHg in the gas experiment.

REFERENCES

- Forum of International Respiratory Societies and European Respiratory Society, The Global Impact of Respiratory Disease, 2017.
- [2] CDC, "CDC Virtal Signs Asthma in the US," May 2011. [Online]. Available: https://www.cdc.gov/vitalsigns/asthma/index.html
- [3] "Chronic Obstructive Pulmonary Disease (COPD) | CDC," Mar. 2021.[Online]. Available: https://www.cdc.gov/copd/index.html
- [4] S. Reuter, C. Moser, and M. Baack, "Respiratory Distress in the Newborn," *Pediatr Rev*, vol. 35, no. 10, pp. 417–429, Oct. 2014.
- [5] I. Costanzo, D. Sen, U. Guler, and L. Rhein, "Respiratory monitoring: Current state of the art and future roads," *IEEE Reviews in Biomedical Engineering*, vol. 15, pp. 103–121, Nov. 2020.
- [6] M. Hernandez-Silveira, K. Ahmed, S.-S. Ang, F. Zandari, T. Mehta, R. Weir, A. Burdett, C. Toumazou, and S. J. Brett, "Assessment of the feasibility of an ultra-low power, wireless digital patch for the continuous ambulatory monitoring of vital signs," *BMJ Open*, vol. 5, no. 5, p. e006606, May 2015.
- [7] I. Costanzo, D. Sen, J. Adegite, P. M. Rao, and U. Guler, "A Noninvasive Miniaturized Transcutaneous Oxygen Monitor," *IEEE Transactions on Biomedical Circuits and Systems*, vol. 15, no. 3, pp. 474–485, Jun. 2021.
- [8] A. Madan, "Correlation between the levels of SpO2 and PaO2," Lung India, vol. 34, no. 3, pp. 307–308, 2017.
- [9] D. C. Hutchison, G. Rocca, and D. Honeybourne, "Estimation of arterial oxygen tension in adult subjects using a transcutaneous electrode." *Thorax*, vol. 36, no. 6, pp. 473–477, Jun. 1981.
- [10] J. D. Tobias, "Transcutaneous carbon dioxide monitoring in infants and children," *Pediatric Anesthesia*, vol. 19, no. 5, pp. 434–444, 2009.
- [11] J. W. Severinghaus, P. Astrup, and J. F. Murray, "Blood Gas Analysis and Critical Care Medicine," Am J Respir Crit Care Med, vol. 157, no. 4, pp. S114–S122, Apr. 1998.
- [12] C.-J. Lim, S. Lee, J.-H. Kim, H.-J. Kil, Y.-C. Kim, and J.-W. Park, "Wearable, Luminescent Oxygen Sensor for Transcutaneous Oxygen Monitoring," ACS Appl. Mater. Interfaces, vol. 10, no. 48, pp. 41026–41034, Dec. 2018.

- [13] I. Costanzo, D. Sen, and U. Guler, "A Prototype Towards a Transcutaneous Oxygen Sensing Wearable," in 2019 IEEE Biomedical Circuits and Systems Conference (BioCAS), Oct. 2019, pp. 1–4.
- [14] I. Costanzo, D. Sen, B. Giri, N. Pratt, P. Rao, and U. Guler, "Fluorescent Intensity and Lifetime Measurement of Platinum-Porphyrin Film for Determining the Sensitivity of Transcutaneous Oxygen Sensor," in 2020 IEEE International Symposium on Circuits and Systems (ISCAS), Oct. 2020, pp. 1–5.
- [15] I. Costanzo, D. Sen, and U. Guler, "An Integrated Readout Circuit for a Transcutaneous Oxygen Sensing Wearable Device," in 2020 IEEE Custom Integrated Circuits Conference (CICC), Mar. 2020, pp. 1–4.
- [16] T. Tufan and U. Guler, "A Fluorescent Thin Film-Based Miniaturized Transcutaneous Carbon Dioxide Monitor," *IEEE Biomedical Circuits and Systems Conference (BioCAS 2021)*, Oct. 2021.
- [17] M. M. Baker, A. Schwindt, and T. Bisdas, "Potential Utility of Tissue Oxygen Sensors in Perfusion | Profusa, Inc." May 2018. [Online]. Available: https://profusa.com/publication/potential-utility-oftissue-oxygen-sensors-in-perfusion-monitoring-miguel-montero-bakermd-arne-schwindt-md-and-theodosios-bisdas-md-phd/
- [18] S. Sonmezoglu, J. R. Fineman, E. Maltepe, and M. M. Maharbiz, "Monitoring deep-tissue oxygenation with a millimeter-scale ultrasonic implant," *Nat Biotechnol*, vol. 39, no. 7, pp. 855–864, Jul. 2021.
- [19] M. Quaranta, S. Borisov, and I. Klimant, "Indicators for Optical Oxygen Sensors," *Bioanalytical reviews*, vol. 4, pp. 115–157, Dec. 2012.
- [20] "CN0503 Circuit Note | Analog Devices." [Online]. Available: https://www.analog.com/en/design-center/reference-designs/circuits-from-the-lab/cn0503.html#rd-overview
- [21] "Cutaneous Carbon Dioxide (PcCO2) and Oxygen (PcO2) Monitors - Class II Special Controls Guidance Document for Industry and FDA," Mar. 2021. [Online]. Available: https: //www.fda.gov/medical-devices/guidance-documents-medical-devicesand-radiation-emitting-products/cutaneous-carbon-dioxide-pcco2-andoxygen-pco2-monitors-class-ii-special-controls-guidance-document